scientific reports

Check for updates

OPEN

Experimental analysis of the damping characteristics of longmaxi shale under graded cyclic loading with different confining pressures

Jiajun Shu[1,2,3]✉, Tao Li[1,2]✉, Yue Li[1,2], Bingni Wu[5], Zhengding Deng[4], Jingzhu Huang[4], Fausto Molina-Gómez[3] & Rubén Galindo[3]✉

In the process of shale gas field development, the surrounding rock has been in a three-way high-pressure stress state for a long period of time and has undergone complex cyclic loading during hydraulic fracturing and high-pressure fracturing fluid return, and its mechanical response and mechanism of action have important impacts on the stability of the reservoir. To reveal the damping characteristics of Longmaxi shale under different peripheral pressures, graded cyclic loading tests were carried out under 0 MPa, 10 MPa and 30 MPa peripheral pressures to systematically analyze the stress–strain hysteresis characteristics of the shale and the evolution of the damping ratio. The results show that the damping ratio of the Longmaxi shale shows a staged evolution with increasing stress level, which is characterized by "decreasing, stabilizing, and then slightly increasing". During cyclic loading, the axial and radial damping ratios both decreased and stabilized with increasing number of cycles. The radial damping ratio was always greater than the axial damping ratio under the same circumferential pressure conditions, and the difference was more significant under high circumferential pressure conditions. Shale exhibits typical characteristics of hysteresis and damping response evolution during dynamic loading, reflecting a progressive phase shift wherein strain increasingly lags behind stress. This phenomenon primarily arises from the accumulation of plastic deformation, the continuous propagation of microfractures, and the sequential activation of multistage energy dissipation mechanisms. The damping ratio follows a staged evolution pattern characterized by an initial decline, a period of stability, and a final surge. This trend indicates a transition in the material's response mechanism—from being dominated by structural compaction to being governed by microscopic damage processes.

Keywords Longmaxi shale, Confining pressures, Graded cyclic loading, Damping characterization, Hysteresis curve

Oil and gas resources are not only the main source of energy for the daily operation of human society and the main raw material for chemical production but also important national strategic materials. As a major global consumer of oil and gas resources, the demand of China for oil and gas has shown a changing trend of year-to-year growth. In the context of the current development of resource extraction in China, continuous large-scale exploitation over the past decade has led to the depletion of shallow mineral and hydrocarbon resources, and current resource extraction methods have gradually reached depths of 3000–4000 m[1,2]. Important production bases for petroleum and petrochemicals, such as China's Chuannan shale gas field, the Chongqing Fuling shale gas field and the Hubei Jianghan oil field, not only occupy important positions in the history of oil and gas

[1]Inner Mongolia Research Institute, China University of Mining & Technology-Beijing, Ordos 017000, China. [2]School of Mechanics and Civil Engineering, China University of Mining and Technology-Beijing, Beijing 100083, China. [3]Higher Technical School of Civil Engineers, Universidad Politécnica de Madrid, 28039 Madrid, Spain. [4]School of Civil and Surveying & Mapping Engineering, Jiangxi University of Science and Technology, Ganzhou 341000, China. [5]School of Civil Engineering and Architecture, East China Jiaotong University, Nanchang 330013, China. ✉email: shujj98@qq.com; litcumt@163.com; rubenangel.galindo@upm.es

resource development but also play key roles in the current development of unconventional oil and gas resources and energy transformation. Among them, the Jianghan Oilfield is dominated by land-phase sedimentary oil and gas reservoirs and has typical geological characteristics of fracture basins. After decades of high-intensity exploitation, some reservoirs have entered the middle and late stages of development, and the Jianghan Oilfield is facing problems such as resource depletion and a low recovery rate. Therefore, the development of unconventional oil and gas resources has gradually become the focus of research and development in the field. Currently, the Jianghan Oilfield has made some progress in the development of tight oil, shale gas and other unconventional resources, and the application of related technologies is expected to further increase the oil and gas recovery rates and extend the production life cycle of the field[3–5].

Deep shale reservoirs typically exhibit low porosity and low permeability under high confining pressures, high temperatures, and complex stress conditions; thus, most drilled wells rely on hydraulic fracture modifications to improve reservoir permeability. During the drilling modification and hydrocarbon extraction process, the shale reservoir and surrounding borehole rock are subjected to long-term cyclic loading, including drilling-induced vibrations, periodic pressure fluctuations induced by hydraulic fracturing, and the continuous evolution of in situ stress. The damping effect, as a mechanism for the dissipation of external disturbance energy in rock masses, directly influences fracture propagation dynamics, fluid transport behavior, and the long-term stability of the reservoir. During the hydraulic fracturing process, the damping characteristics determine the stress release rate at the fracture tip and the energy dissipation pattern. Higher damping stabilizes fracture propagation, reducing the risk of sudden failure, whereas low-damping shale is more prone to dynamically unstable fracture growth, which may lead to an uncontrolled fracture network morphology and even borehole instability. During the fluid transport process, the damping effect regulates the dynamic opening and closing of fractures, influencing the evolution of reservoir permeability. High-damping shale dissipates fluid-driven energy to maintain the fracture aperture, enhancing the stability of flow pathways, whereas low-damping rock is more susceptible to fracture closure, leading to hindered fluid flow. In the long term, damping plays a critical role in the evolution of fatigue damage in rock masses by dissipating the strain energy accumulated from cyclic loading. This helps delay the deterioration of the reservoir, mitigate borehole instability, and suppress geological deformation. The evolution of the damping properties directly affects the deformation response, fracture expansion, and mechanical stability of the reservoir, which in turn affects extraction safety[6–8]. The damping properties of rocks usually refer to their ability to dissipate energy under external forces, which mainly involve internal friction energy dissipation, viscous dissipation and energy dissipation processes induced by fissure extension. Among them, internal friction energy dissipation originates from relative slip and rearrangement between mineral particles, viscous energy dissipation is affected mainly by the viscoelasticity of the pore fluid, and energy loss due to fissure extension reflects the damage evolution characteristics of the rock[9,10]. Previous studies have shown that the damping properties of rocks are significantly affected by external stress conditions[11]. Under a certain confining pressure environment, the deformation response of rock is more stable than that without confining pressure, and fracture extension is suppressed to a certain extent, thus reducing energy dissipation[12,13]. Under cyclic loading, the microcracks and pore structures within rock are continuously rearranged, resulting in gradual energy dissipation and leading to a gradual increase in the damping ratio[14,15]. This means that there is a significant difference in the mechanical response of the rock under different loading modes, and this difference ultimately manifests as a difference in the macroscopic damping characteristics.

In recent years, research on the damping characteristics of deep rock has gradually increased, and important progress has been made in understanding the formation mechanism of rock damping, which is usually categorized into two major categories: internal friction damping and structural damping. Among them, internal friction damping is mainly controlled by the friction between mineral grains within rock and the emergence and expansion of microcracks, whereas structural damping is closely related to the overall structural characteristics of rock, including the effects of fractures, laminations and their interactions on energy dissipation[16,17]. In subsequent studies, scholars initially modeled the quantitative relationship between rock damping properties and factors such as rock type, strain amplitude, and frequency through large theoretical analyses and experimental studies[18–20]. Moreover, the application of numerical simulation methods in deep rock damping research has been widely developed and is based on advanced numerical simulation techniques such as the finite element method and the discrete element method, which can effectively simulate the damping characteristics of rocks under complex dynamic loads[21,22]. In addition, with the continuous progress of high-performance computing technology, multiscale and multiphysics field coupled simulations of rock damping have been explored more deeply.

Despite the remarkable progress in research on rock damping properties, many shortcomings and challenges remain. The effects of the microstructural characteristics of rock, a complex multiphase material, on damping properties have not been fully revealed. There is still a lack of sufficient experimental data and theoretical modeling support on how factors such as microcracks, porosity, and mineral composition within rock affect the energy dissipation process[23,24]. Most existing experimental studies are conducted in laboratory environments, which, while providing valuable data on the physical and mechanical properties of rock masses, often overlook the complex interaction between deep-seated stress and damping effects. In deep underground environments, the effects of high temperature, high pressure, and deep-seated stress on rock masses differ significantly from those under laboratory conditions. These factors not only influence the mechanical properties of rock but also significantly alter its damping characteristics. In the deep stress field, the anisotropy, fracture network, and microstructure of rock masses significantly affect wave propagation and energy dissipation, which is difficult to simulate fully under laboratory conditions. Furthermore, in deep environments, cyclic loading, fluid pressure, and temperature variations further influence the damping effect of rock masses. In particular, under long-term dynamic loading, the relationship between multistage cyclic loading and the damping characteristics of rock masses has not been fully explored. The mechanical behavior of deep rocks is subject to a combination of

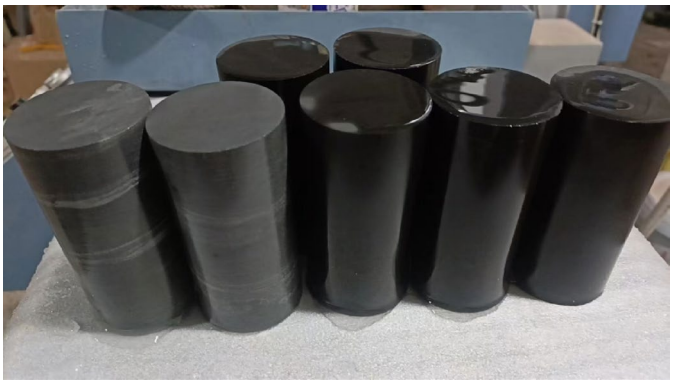

Fig. 1. Longmaxi shale specimens.

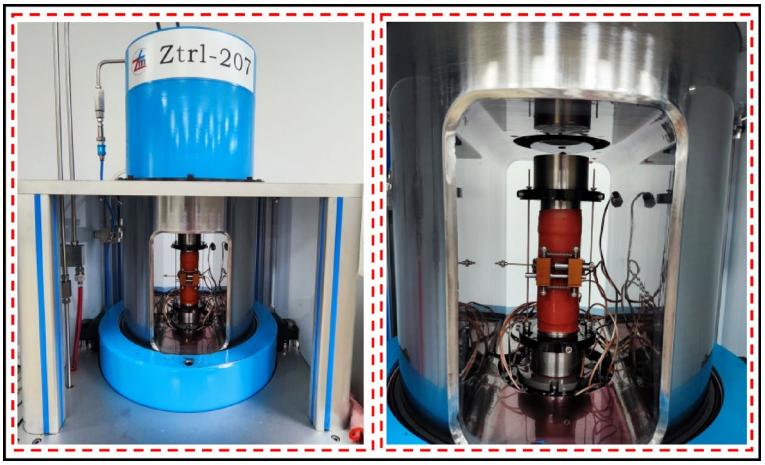

Fig. 2. Ztrl-207 Rock triaxial mechanical tester.

factors, such as temperature, pressure, water content, and other environmental conditions, which are difficult to reproduce adequately in the laboratory[25,26]. On the other hand, although numerical simulation techniques play an important role in rock damping research, the accuracy of their models and computational methods is highly dependent on the support of experimental data, and the available experimental data are not yet sufficient to support more complex numerical simulation models, which limits the accuracy and reliability of some simulation results. To further understand the deformation characteristics and damping evolution of Longmaxi shale under complex stress paths, this paper will carry out variable upper and lower limits of equal-amplitude graded cyclic loading tests under different circumferential pressure conditions to analyze the shale deformation, hysteresis, and damping characteristics in different directions, which is aimed at providing important references for the design and construction of underground shale reservoirs.

Overview of the test

Specimens and equipment

The Longmaxi shale samples used in this study were taken from the subsurface of the Jianghan Basin in Hubei Province, China, at a depth of approximately 3500 m, which is a tight unconventional oil and gas reservoir. To ensure the high quality of the test results, conventional coring techniques were used for subsurface core collection to ensure the integrity of the cores. During coring, directional drilling equipment was used to accurately extract cores from specific shale formations to minimize interference with subsequent tests due to cracks or stress release effects that may occur during the drilling process. After core retrieval, the samples were cleaned to remove surface contaminants and drilling fluid residues. Then, they are sealed and stored with specialized sealing materials such as polyurethane foam, silicone and epoxy resin. In the sample preparation stage, the core was processed into a standard column specimen with a diameter of 50 mm and a height of 100 mm. To ensure that the surface flatness and perpendicularity of the sample met the experimental requirements, the sample preparation process strictly followed the technical specifications of the International Society for Rock Mechanics (ISRM), and the processed sample is shown in Fig. 1.

The equipment used for the test was a ZTRL-207 rock triaxial mechanical tester, as shown in Fig. 2. The equipment consists of a computer and an automatic digital control system, which is capable of real-time

acquisition of mechanical parameters such as load, stress, displacement and strain in the testing process and synchronously generates stress-strain curves. The equipment has an axial loading capacity of up to 7000 kN, an axial displacement range of -50 mm to 50 mm, and a maximum confining and permeability pressure of 70 MPa. The control mode of vibration loading includes two kinds of axial load control and axial displacement control. The vibration waveform can be set as a sine wave, triangle wave, square wave, oblique wave or random wave, and different waveforms, frequencies and phases can be adjusted according to the test requirements. During the test, the microcomputer signal generator board generates a given signal, which is amplified by a power amplifier and input into the host computer to drive the vibration loading. The vibration signal is collected by the sensor and transmitted to the dynamic strain amplifier, which is fed back and stored in the microcomputer through the data acquisition board to finalize the data processing and analysis.

Test program

Different confining pressures were applied to the shale samples via a ZTRL-207 Rock triaxial mechanical tester, and the confining pressure levels were set at 0 MPa, 10 MPa and 30 MPa. The axial load was subsequently applied according to a cyclic stress. The load application was in axial stress control mode, with a sinusoidal loading waveform and a loading frequency of 0.2 Hz. At the first stress level, the minimum axial stress was set as a proportion of 10% of the average compressive strength of the shale under the corresponding circumferential pressure conditions; in the subsequent loading process, the upper limit of each stress level was increased by 10 MPa, and 200 cycles were carried out at each stress level. The specific loading path is shown in Fig. 3.

The damping ratio of rock reflects energy dissipation due to internal friction caused by sliding of the cleavage surface and fluid viscosity under cyclic loading, which reveals the characteristics of the internal energy dissipation of rock under dynamic cyclic loading. The Longmaxi shale, as a typical nonideal elastic body, forms a plastic hysteresis loop between the dynamic stress and dynamic strain under graded cyclic loading, as shown in Fig. 4. In the figure, σ_{max} and σ_{min} denote the maximum and minimum stresses in the hysteresis loop, respectively, and ε_{max} and ε_{min} min denote the maximum and minimum strains in the hysteresis loop, respectively. The hysteresis circle is enclosed by points A, B, C, and D, where point A is the highest point of the hysteresis circle, point C is the lowest point, and point E is the midpoint of the line connecting points A and C (i.e., the straight line AC). An X-axis parallel line is made through point E, which intersects the hysteresis curve at points B and D, and an X-axis vertical line is made through point A to intersect the straight line BD at point E[27–30].

From the area enclosed by the curves in the stress-strain hysteresis loop and through Eq. (1), the damping ratio of the shale under cyclic loading conditions can be calculated. When the rock is subjected to cyclic loading, not only is the axial direction deformed but also the radial direction is deformed. These data were obtained by loading the equipment in Fig. 2. Therefore, the plastic hysteresis effect between the radial strain and axial stress is also exhibited, i.e., both the axial damping ratio and the radial damping ratio can be calculated via Eq. (1).

$$\lambda = \frac{A_R}{4\pi A_S} \tag{1}$$

where A_R is the area of the hysteresis loop ABCD, reflecting the size of the energy dissipated by the rock sample due to intrinsic damage in a cyclic process, the area of the hysteresis loop is calculated by solving the trapezoidal area superposition via the microelement method in data processing. A_S is the area of the triangle AEF.

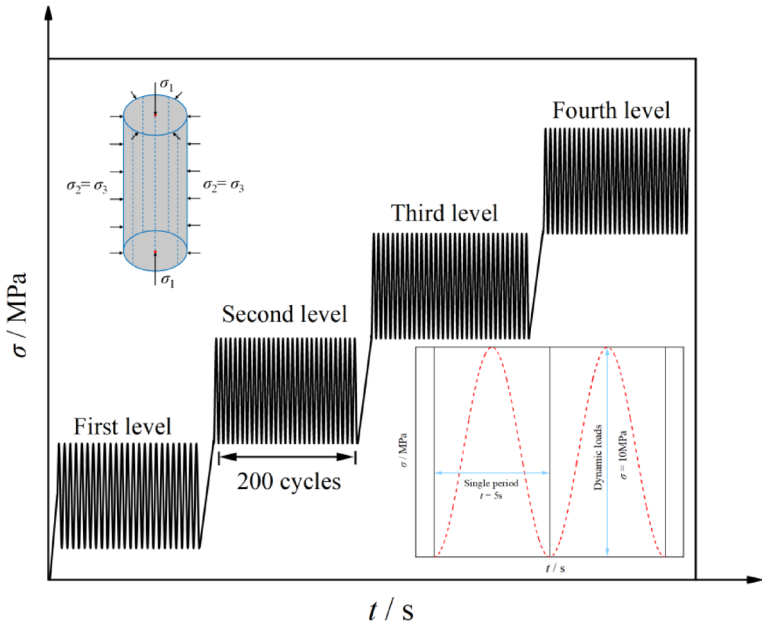

Fig. 3. Stress loading path diagram.

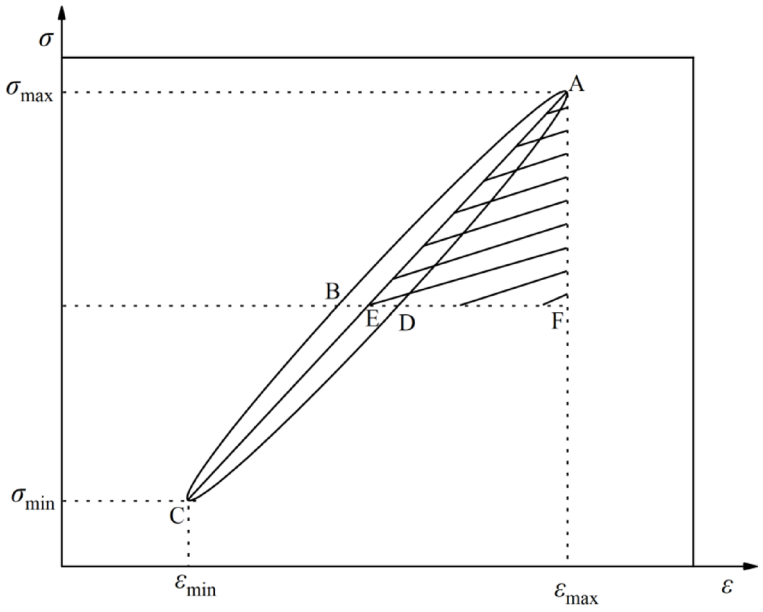

Fig. 4. Stress–strain hysteresis loop.

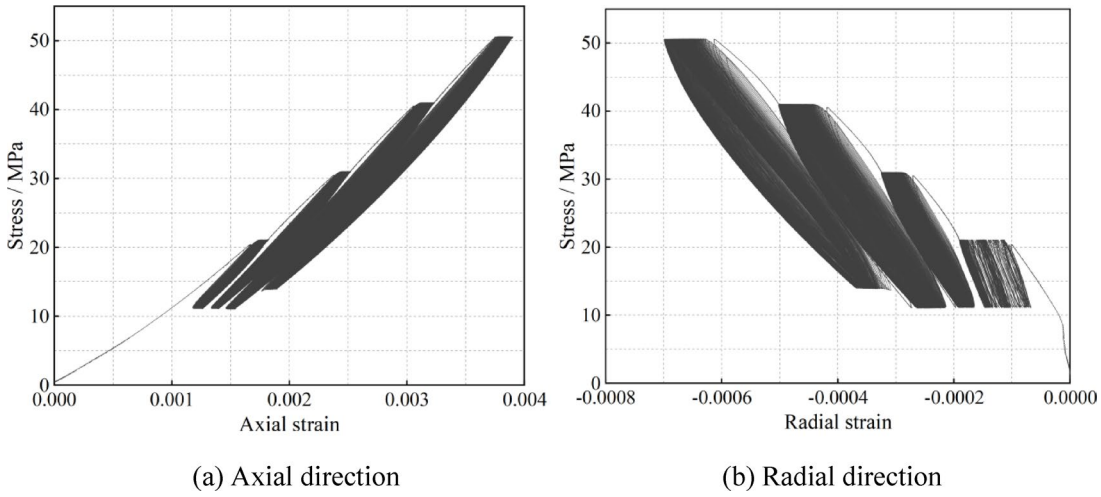

Fig. 5. Stress–strain hysteresis loop at a confining pressure of 0 MPa.

Test results and analysis

Stress–strain hysteresis

The stress–strain curves under equal-amplitude cyclic loading with different upper and lower limits of pericompression variations are shown in Fig. 5, 6 and 7.

Figures 5, 6 and 7. show two types of stress–strain hysteresis curves of Longmaxi shale under equal-amplitude cyclic loading in both the axial and radial directions at radial pressures of 0 MPa, 10 MPa and 30 MPa, respectively. At an enclosing pressure of 0 MPa, the shale is virtually unconfined laterally, and the internal mineral grains are more loosely connected to each other. During cyclic loading, the stress–strain hysteresis curve shows a narrower and longer pattern. This is because, owing to the loading process, relative slip and misalignment between the mineral particles are more likely to occur, resulting in a rapid increase in strain; in the unloading stage, owing to the lack of sufficient binding force to inhibit particle rebound, the elastic deformation of the material can be recovered faster but is still accompanied by a certain amount of residual plastic deformation. With increasing number of cycles, plastic deformation gradually accumulated, and the hysteresis loop was offset. When the peripheral pressure was increased to 10 MPa, the shale was subjected to significant lateral constraints, and the interaction force between the particles increased, limiting the occurrence of particle slip and misalignment. Therefore, at the same strain level, the material needs to be subjected to greater stress, which is manifested by an increase in the slope of the hysteresis curve. The increase in the peripheral pressure also caused the free springback of the particles in the unloading stage to be suppressed and the hysteresis loop to become fuller,

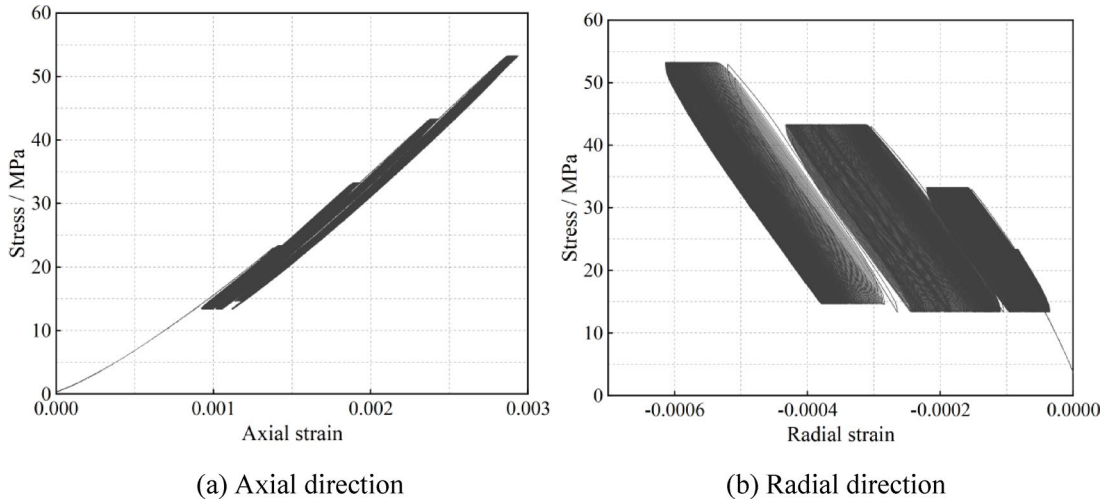

Fig. 6. Stress–strain hysteresis loop at a confining pressure of 10 MPa.

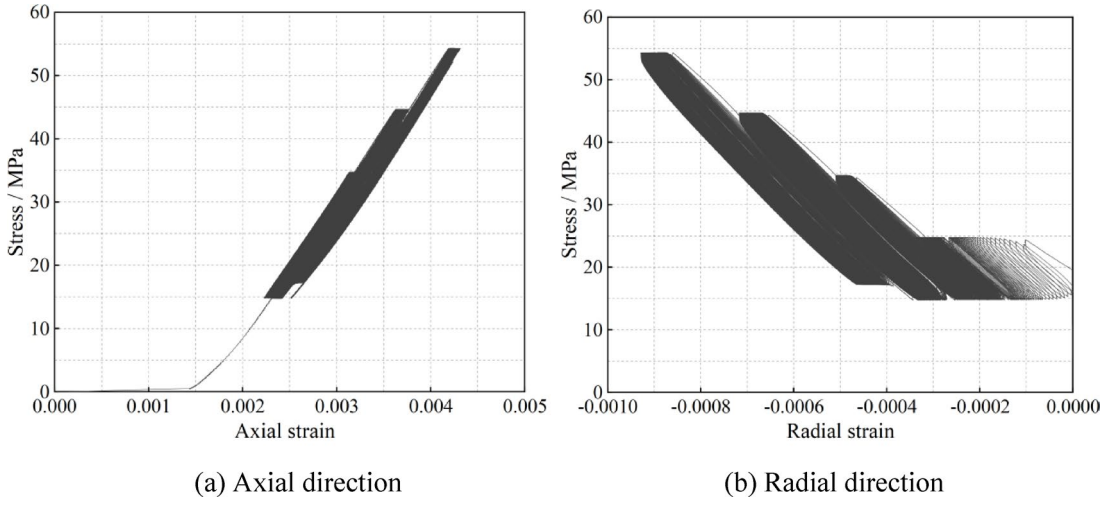

Fig. 7. Stress–strain hysteresis loop at a confining pressure of 30 MPa.

indicating an increase in the energy dissipation of the material during cyclic loading, whereas the rate of accumulation of plastic deformation slowed down compared with that at 0 MPa peripheral pressure. When the peripheral pressure is further increased to 30 MPa, the lateral constraints imposed on the shale significantly increase, leading to significant changes in the deformation mechanism of the internal structure. High peripheral pressures not only limit the relative slip of mineral particles but also may contribute to particle fragmentation and plastic flow, leading to a nonlinear stress–strain relationship, which may be accompanied by the occurrence of radial damage.

When the axial strain reaches 0.0025, the corresponding upper and lower stress limits of the shale samples are 22.91–30.02 MPa, 42.41–44.99 MPa, and 16.45–20.87 MPa under confining pressures of 0 MPa, 10 MPa, and 30 MPa, respectively. These results indicate that the confining pressure significantly influences the dynamic modulus of shale, with a clearly staged effect: moderate confining pressure enhances the dynamic modulus, whereas excessive confining pressure leads to a reduction in the dynamic modulus. At low to moderate confining pressures (0–10 MPa), the external pressure effectively suppresses the lateral expansion of the shale during cyclic loading and restricts the opening of primary pores and microfractures. This promotes the closure of microcracks and increases the compactness of the material, thereby increasing its capacity for load transfer. During this stage, the shale structure becomes more compact, and the internal stress distribution is more uniform, leading to an increased dynamic modulus and a broader stress response range. However, when the confining pressure continues to rise to high levels (e.g., 30 MPa), the intensification of the triaxial compressive stress may induce microstructural degradation phenomena, including particle breakage, interfacial slip between mineral grains, and delamination along weak planes—even though some microcracks may still remain closed. This duality suggests that while the confining pressure enhances the dynamic modulus through physical compaction and partially mitigates structural deterioration under cyclic loading, excessive pressure may lead to irreversible

microstructural damage. Consequently, the mechanical properties of the material are degraded, reflecting a typical "strengthening–weakening" dual regulation effect of confining pressure on shale.

From the point of view of the fine-scale damage mechanism, under lower circumferential pressure conditions, the internal structure of shale is looser, the relative movement between mineral particles is more significant, and plastic deformation develops more quickly. With increasing confining pressure, the shale structure is gradually enhanced due to the increase in material stiffness, which increases energy dissipation and decreases plastic deformation. This results in significant changes in the characteristics of the stress-strain hysteresis curve. Specifically, under nonperipheral-pressure conditions, cyclic loading tends to lead to the emergence and rapid expansion of microcracks within the material, which accelerates the accumulation of plastic deformation and causes the hysteresis curve to exhibit strong instability. Under a certain peripheral pressure, the lateral constraint can effectively inhibit the expansion of microcracks and slow the deterioration process of the internal structure of the material so that, under the same number of cycles, the cumulative amount of plastic deformation is smaller than that of the nonperipheral-pressure condition, and the hysteresis curve tends to stabilize. With a further increase in the peripheral pressure, the stronger lateral constraint may further stimulate the emergence and expansion of microcracks, increasing the dissipation of shale.

Under cyclic loading conditions, the plastic deformation within the shale material gradually accumulates, leading to a progressive phase change in the strain response. This phenomenon is characterized by the strain phase increasingly surpassing the stress phase. During the initial stages of the cyclic loading test, when the loading amplitude is small, the material primarily undergoes elastic deformation, and the stress and strain remain largely synchronized. However, as the loading stress amplitude increases and the number of cycles progresses, irreversible plastic deformation begins to develop within the material. This results in the accumulation of plastic strain energy, which, in turn, induces the evolution of the phase difference between stress and strain. The formation mechanism of this phenomenon can be analyzed in depth from several perspectives. During the loading phase, plastic deformation causes the stress-strain path to deviate from the ideal linear elastic behavior, resulting in the formation of a typical hysteresis loop. In the unloading phase, the unloading path does not coincide with the loading path because part of the plastic strain energy remains unreleased, leading to noticeable stress-strain hysteresis. This energy dissipation and path deviation effect causes the strain response to increase more rapidly than the stress during subsequent loading, thus manifesting as a macroscopic phase shift where the strain phase precedes the stress phase.

Moreover, the shape of the hysteresis loop was found to be downconvex in both the loading and unloading phases, which indicated that there was significant hysteresis between the stress and strain. By observing the shapes of the two types of hysteresis curves, it can be found that the shapes of the radial hysteresis loops are basically the same as those of the axial hysteresis loops, i.e., the radial stress-strain hysteresis relationship is similar to that in the axial direction. Since the hysteresis loop shape can effectively reflect the stress-strain hysteresis relationship, the cycles of the first and fourth loading stages when the enclosing pressure is 0 MPa and the cycles of the fourth loading stage when the enclosing pressure is 10 MPa and 30 MPa are selected for normalization, and the results are shown in Fig. 8. The specific stress and strain normalization calculation procedure is shown in Eq. (2).

$$\begin{cases} \eta_\sigma = \dfrac{\sigma_i - \min\sigma_i}{\max\left[\sigma_i - \min\sigma_i\right]} \\ \eta_\varepsilon = \dfrac{\varepsilon_i - \min\varepsilon_i}{\max\left[\varepsilon_i - \min\varepsilon_i\right]} \end{cases} \tag{2}$$

where η_σ and η_ε are the stresses and strains after normalization and where σ and ε are the stresses and strains before normalization.

Figure 8 shows the normalized stress-strain hysteresis relationship curves under different loading conditions. The figure shows that the normalized stress-strain curves of the shale samples synchronized the stress and strain phases at the early stage of loading during the first stage of loading, with a peripheral pressure of 0 MPa. However, with increasing stress amplitude, the phenomenon of the strain phase exceeding the stress phase occurs in the late loading stage. The stress-strain hysteresis effect diminished as the circumferential pressure increased to 10 MPa; instead, the hysteresis phenomenon became more significant when the confining pressure was further increased to 30 MPa. This phenomenon can be attributed to a combination of stress amplitude and cyclic accumulation effects. At the beginning of loading, the stresses and strains remain synchronized as the material is in the elastic dominant phase. As the stress amplitude and number of cycles increase, plastic deformation gradually accumulates, and the process of storing and releasing plastic strain energy gradually becomes hysteretic, resulting in the strain phase exceeding the stress phase. This is because the plastic strain energy accumulated during the unloading phase is released in hysteresis, which affects the subsequent loading phase, causing the strain phase to overshoot the stress phase during subsequent loading. Unlike the results of Wang et al.[31] concerning the damping ratios of sandstones and shales with viscoelasticity, the hysteresis properties of shales significantly differ in terms of their hysteresis effects. In particular, the phenomenon in which their strain phase generally exceeds the stress phase is similar because of the relative aspects of the hysteresis behaviors of conventional rock materials, suggesting that shales have a unique mechanical response under complex loading conditions[32,33].

The evolution of the stress-strain phase difference is closely related to the microstructural response within the shale. Under cyclic loading, microplastic mechanisms, such as the initiation and propagation of microcracks, intergranular slip, and localized disruption of the contact interface, are continuously activated. These mechanisms not only reduce the local stiffness but also significantly increase the energy dissipation capacity of the material, thereby increasing the asynchrony between the stress and strain responses. Specifically, as the number of cycles

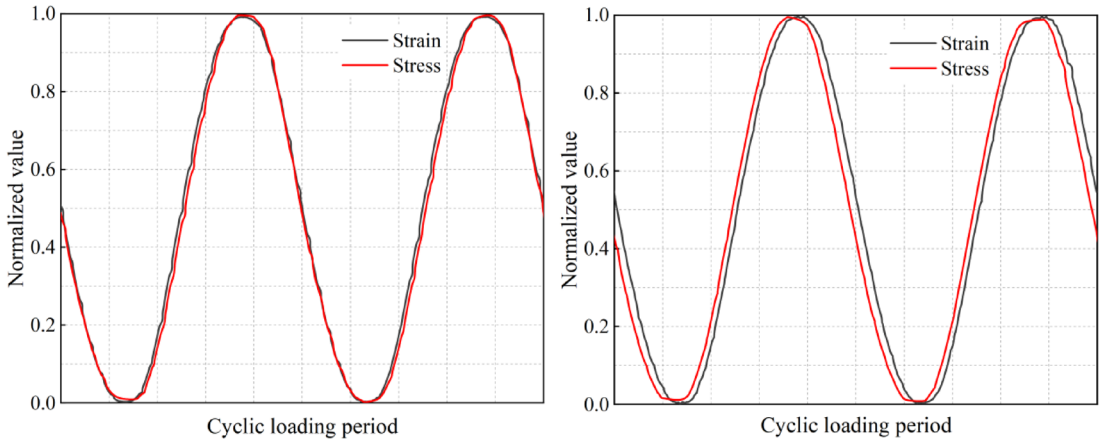

(a) First-level loading (0 MPa confining pressure) (b) Fourth-level loading (0 MPa confining pressure)

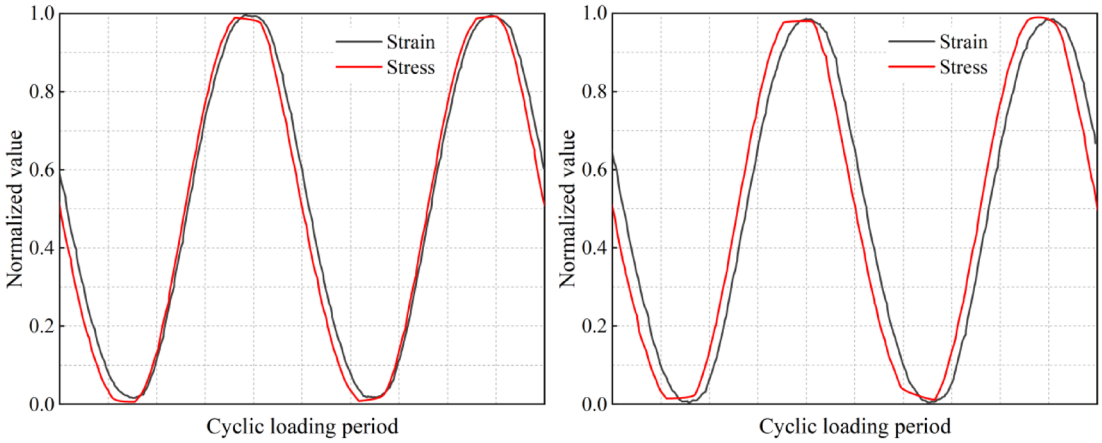

(c) First-level loading (10 MPa confining pressure) (b) Fourth-level loading (30 MPa confining pressure)

Fig. 8. Stress–strain hysteresis relationship after normalization.

increases, microscopic damage accumulates within the material, leading to a gradual degradation of its overall mechanical properties and further weakening the coupling between stress and strain. Macroscopically, this process is reflected by the expansion of the hysteresis loop area and changes in damping characteristics, which indicate a dominant increase in inelastic energy dissipation. The continuous evolution of the microstructure and the accumulation of damage jointly drive the kinetic response, where the strain phase progressively overtakes the stress phase. This reveals the underlying basis and microscopic mechanisms behind the formation and development of the stress–strain phase difference.

Damping characteristics

Figures 9, 10 and 11 illustrate the changes in the axial and radial damping ratios of the shale samples as a function of the number of cycles under different loading levels and enclosing pressures of 0 MPa, 10 MPa, and 30 MPa. The evolution curve of the axial damping ratio is presented on the left side of each figure, whereas the trend of the radial damping ratio is shown on the right. The horizontal axis represents the number of cycles (with a total of 200 cycles), and the vertical axis represents the corresponding damping ratio values. These figures reflect the dynamic response behavior of the sample throughout the entire loading process.

Figure 9 shows that, under the condition of no peripheral pressure (0 MPa), both the axial and radial damping ratios clearly decay, particularly in the first 20 cycles, where the decay is more pronounced. Afterward, the damping ratios gradually stabilize, with some variation in the damping response observed at different loading levels. Figure 10 presents the results under a 10 MPa enclosing pressure. While the overall evolution trend still follows a "fast then slow" decay pattern, the damping ratios are slightly lower than those under the 0 MPa condition, and the curve changes more smoothly. Figure 11 shows the response at 30 MPa, where the damping

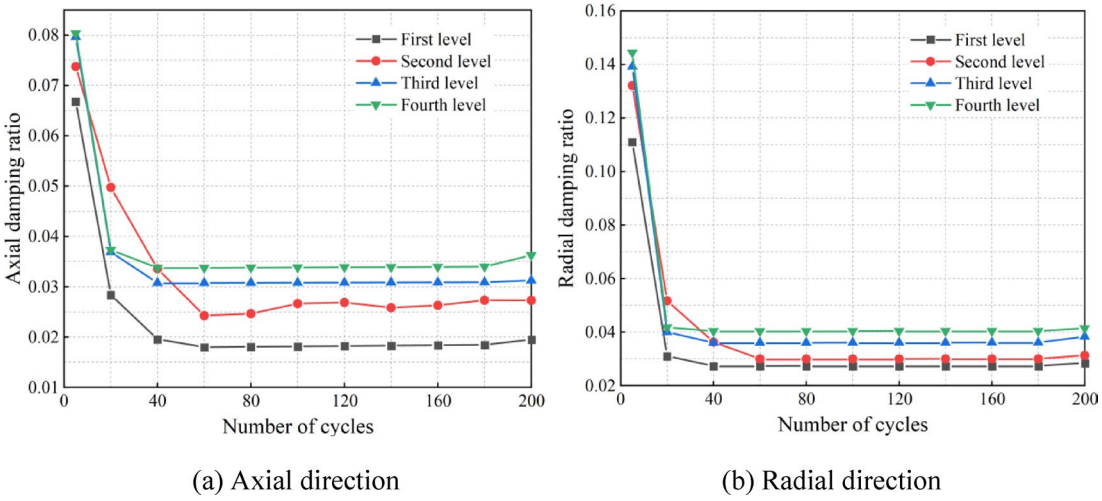

(a) Axial direction (b) Radial direction

Fig. 9. Damping ratio of shale at a confining pressure of 0 MPa.

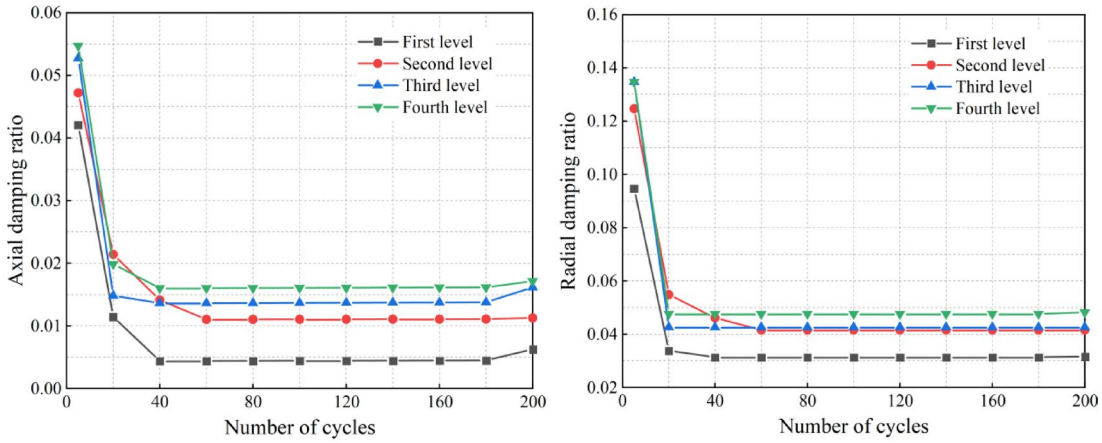

(a) Axial direction (b) Radial direction

Fig. 10. Damping ratio of shale at a confining pressure of 10 MPa.

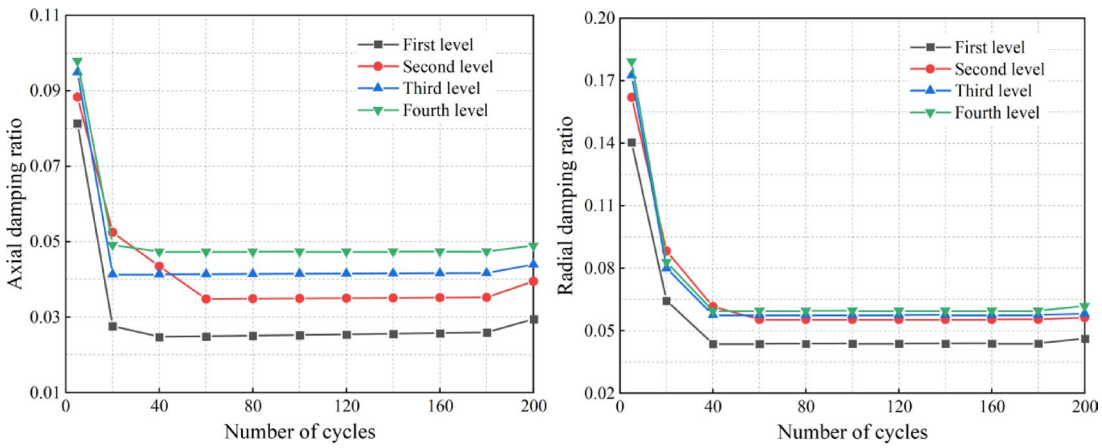

(a) Axial direction (b) Radial direction

Fig. 11. Damping ratio of shale at a confining pressure of 30 MPa.

ratios are significantly lower than the initial values. The amplitude of variation with the number of cycles further decreases, and the damping curve overall shows a smoother and slower change.

According to the change curves of the damping ratio in Figs. 9, 10 and 11, the damping ratio of the Longmaxi shale sample clearly changes with increasing stress level (i.e., the upper and lower limits of the stress gradually increase). In the initial stage, the damping ratio gradually decreases and tends to lower values as the stress level increases. However, the damping ratio tends to increase when the stress loading level further increases. In addition, the damping ratio of the first cycle is usually the largest at the same stress level. This is attributed to the increase in the upper stress limit, leading to new damage inside the shale, which triggers greater deformation and energy dissipation. During the following cycles, the damping ratio gradually decreases and stabilizes. As the stress loading level increases, its stabilization value is lower than that at lower stress levels. This pattern of change is consistent with the evolution trend of the damping ratio under the action of step-by-step loading, i.e., the damping ratio first decreases, then tends to stabilize, and ultimately increases slightly.

A comparison of the axial and radial damping ratios reveals that the radial damping ratio of shale is always greater than its axial damping ratio under the same circumferential pressure and stress loading conditions, and this difference is more significant under higher circumferential pressure conditions. This phenomenon can be attributed to the evolution of microfractures inside the shale. In the initial stage, the sample contains many microfractures and pores inside the sample, and as the stress level increases and the number of cycles increases, the microstructure gradually densifies, leading to a gradual decrease in energy dissipation, which results in a decrease in the damping ratio. When the upper and lower stress limits reach a certain level and undergo a sufficient number of cycles, the shale enters the dominant phase of elastic deformation, and the role of viscous forces between mineral particles is weakened, resulting in a decrease in the magnitude of the variation in the damping ratio, especially in the subsequent cycling stages except for the first cycle, where the damping ratio gradually tends to stabilize.

During the graded cyclic loading process, the damping ratios of the shale samples exhibit typical stage-by-stage evolution with the number of cycles. In the initial loading stage, the primary pore and microfracture structures in the shale are not significantly disturbed. Under conditions of low stress amplitude and a limited number of cycles, the repeated loading–unloading actions cause some pores and cracks to undergo compressive closure. This leads to densification of the internal structure and a gradual reduction in energy dissipation, which is reflected as a significant decrease in the damping ratio as the number of cycles increases. In this stage, the damping behavior is governed primarily by viscous energy dissipation from pore compression and weak friction at microfracture surfaces. The damping mechanism is thus dominated by low-intensity interfacial slip and contact friction.

In the middle stage, as the number of cycles continues to increase, the shale exhibits typical quasielastic response characteristics. With the main pores and cracks stabilizing in a closed state, the structural compaction effect diminishes. The material's overall deformation becomes predominantly elastic, and the energy dissipation capacity stabilizes. Consequently, the damping ratio decreases in response to the number of cycles, and the curve fluctuates gradually. At this stage, the energy dissipation induced by cyclic loading is more limited, and the damping response remains relatively stable because of the small relative slip between mineral particles and the lack of significant redevelopment of the fracture structure.

However, as the number of cycles increases further and approaches the instability stage, the damping ratio significantly increases in the final few loadings. This phenomenon primarily results from the continuous expansion of cracks within the shale as localized microdamage develops. With the ongoing application of external cyclic loading, the material transitions from a macrostructural stable state to a critical, unstable state dominated by microstructural damage. At this stage, microcracks rapidly initiate, expand, and eventually connect, triggering intense slip friction and structural reorganization between particles. This leads to a substantial increase in energy dissipation. At this point, the damping effect not only involves slip friction along the original cleavage interfaces but also includes opening and closing motions and viscous energy dissipation between newly formed cleavage surfaces. These processes result in a sharp increase in the damping ratio's response characteristics.

Overall, the evolution of the damping ratio can be categorized into three phases: initial decrease, middle stability, and final increase. This progression reflects the dynamic response mechanism of shale, which transitions from structural compaction to damage evolution under cyclic loading. Specifically, the increase in the damping ratio at the final stage serves as a sensitive indicator of impending destabilization and damage in the shale samples.

Analysis and discussion

The analysis above reveals that the damping ratio of Longmaxi shale under different pressure conditions evolves in stages with changes in stress levels, characterized by a pattern of "decreasing, stabilizing, and then slightly increasing." This trend is somewhat consistent with established findings on rock damping properties but also highlights the distinct mechanical response behavior of shale materials[34]. Under low confining pressure conditions, the damping ratio gradually decreases as the stress level increases, which aligns with previous studies showing that confining pressure inhibits fracture extension[35]. Specifically, at the initial stage with low stress levels, primary microfractures close and compact under compression, enhancing interparticle contact. This leads to a weakening of inelastic energy dissipation mechanisms such as interfacial friction and slip, resulting in a significant decrease in the damping ratio. However, as the circumferential pressure increases and the stress level continues to rise, the damping ratio begins to rebound, reflecting the significant impact of cyclic loading-induced microfracture redistribution and extension under high-stress conditions. The reactivation of cracks enhances interfacial slip, particle rearrangement, and localized structural damage processes, leading to an increase in the energy dissipation capacity and a subsequent rebound in the damping ratio[36]. This damping evolution process indicates that, under high peripheral pressure, the damping mechanism of shale shifts from being dominated

by fissure closure and structural compaction to being governed by fissure extension and localized damage. Compared with common rocks such as sandstone and chert, Longmaxi shale exhibits notable anisotropic damping characteristics. The radial damping ratio is consistently higher than the axial damping ratio, with this difference being particularly pronounced at high peripheral pressures[37,38]. This behavior is closely related to the significant laminated structure of shale and the directional distribution of microfractures. During cyclic loading, radial deformation is more strongly constrained by peripheral pressure, which facilitates the activation of microscopic energy dissipation mechanisms, such as particle slippage along laminar surfaces and the repeated closure and opening of cracks. This, in turn, enhances the energy dissipation capacity in the radial direction. These features collectively underscore the dominant role of structural damping in the damping properties of shale and provide a microscopic basis for understanding its anisotropic dynamic response characteristics.

From a mechanistic perspective, the damping behavior of rocks is a comprehensive reflection of energy dissipation processes, including internal friction, viscous hysteresis, and fissure extension. For shale, under low peripheral pressure conditions, the connections between internal mineral particles are relatively loose, and significant relative slip occurs between the particles during cyclic loading. In this scenario, internal friction becomes the dominant energy dissipation mechanism, and damping is primarily controlled by slip friction at the contact surfaces of the particles. As the peripheral pressure increases, the lateral constraints are enhanced, significantly suppressing interparticle slip. The viscous drag effect of the fluid in the pore structure begins to emerge, particularly under conditions involving fracturing fluid retention. The pore space undergoes viscoelastic deformation, and the viscous dissipation mechanism becomes dominant, leading to the stabilization of the damping ratio. Interestingly, at high peripheral pressures, the damping ratio tends to increase, indicating the activation of energy dissipation mechanisms associated with fracture extension. At this stage, the internal microstructure of shale subjected to three-way compressive stress becomes more prone to damage, initiating microstructural evolution processes such as particle fragmentation, mineral interface slip, and local plastic deformation. This triggers the formation and expansion of numerous microfractures, significantly enlarging the hysteresis loop and causing the damping ratio to rise again. This indicates a transition in the energy dissipation mechanism from "particle slip dominance" to "fissure expansion dominance"[18,39,40]. In terms of the anisotropic response, the experimental results show that the radial damping ratio is consistently greater than the axial damping ratio. This can be attributed to the fine-grained structural properties of shale: axial loading primarily triggers the rearrangement and compaction of particles along the loading direction, resulting in a relatively simple structural response. In contrast, radial deformation, which is constrained by strong circumferential pressure, is more likely to induce complex processes, such as shear slip along the lamina plane and the repeated closure and opening of fractures[41,42]. These nonlinear processes increase internal friction energy dissipation (e.g., interlayer slip friction) and structural damping (e.g., interfacial damage such as debonding of the laminae) in the radial direction[41,42].

Although this study provides a more systematic understanding of the influence of perimeter pressure on the evolution of shale damping properties through graded cyclic loading tests, there are still significant differences between laboratory test conditions and the actual deep reservoir environment. These differences need to be addressed and expanded upon in future studies, specifically in the following three areas. First, the current experiment does not account for multifield coupling conditions. It focuses solely on the effects of perimeter pressure and axial cyclic loading, neglecting the synergistic effects of other physical fields, such as temperature, pore pressure, and the chemical environment, on shale damping behavior. In real formations, the thermal expansion coefficient differences between various mineral components at high temperatures can alter particle contact states and induce thermally driven fractures, which in turn affect energy dissipation through internal friction. Additionally, dynamic changes in pore pressure (e.g., cyclic seepage due to the injection and discharge of fracking fluids) may cause fractures to repeatedly open and close, thereby increasing viscous energy dissipation. Furthermore, the interaction between fracturing fluids and rock (including mineral dissolution, solvation, etc.) may lead to structural degradation and a decline in mechanical parameters, which would change the energy dissipation mechanisms. Therefore, the current experimental results have limitations in explaining the damping response behavior under complex geological conditions. Second, the loading path used in this study is relatively simplified. The cyclic load is applied in the form of a constant-frequency sinusoidal wave, which does not accurately replicate the complex stress paths encountered during reservoir fracturing and return processes, such as asymmetric loading, frequency changes, and pulsed disturbances. Previous research has shown that the loading frequency significantly influences the viscous energy dissipation mechanisms of materials. Shale exhibits a more pronounced viscoelastic response under high-frequency conditions, potentially leading to mode migration in its damping behavior. Thus, the idealized loading approach in this study may underestimate the influence of frequency on the evolution of the damping ratio in real-world engineering scenarios. Finally, time effects were not fully considered in this experiment. As a typical viscoelastic–brittle composite material, the mechanical response and damping characteristics of shale are highly dependent on parameters such as loading duration and rate. These characteristics are particularly susceptible to hysteresis processes, such as creep and time-dependent damage, under long-term loading or load-holding conditions, which significantly alter the energy dissipation mechanisms and structural evolution paths. However, long-term loading experiments compatible with geological time scales were not conducted in this study, making it difficult to capture the temporal evolution of the damping properties of shale over extended periods[43,44].

A comparative study of the damping characteristics of various rock types revealed that the hysteresis loop curves exhibit an evolution trend characterized by a transition from sparse to dense and then back to sparse throughout the cyclic loading process. This pattern also appears within a single stress level, where the hysteresis loops progressively densify and subsequently loosen. In terms of the phase response, significant differences are noted between mudstone and sandstone. For mudstone, the strain phase is generally synchronized with or slightly lags behind the stress phase during loading but lags more noticeably during unloading, resulting

in a sharp-lobed hysteresis loop. In contrast, sandstone gradually accumulates plastic deformation as both the stress amplitude and the number of cycles increase. This leads to the strain phase surpassing the stress phase, which is indicative of the progressive activation of inelastic energy dissipation mechanisms. The damping ratios in mudstones are generally higher than those in sandstones, and both rock types clearly exhibit anisotropy—specifically, the radial damping ratios are significantly greater than the axial damping ratios. This anisotropic behavior is closely related to the internal laminated structure and the preferential orientation of microfractures. In terms of the cyclic loading response, the relative area and damping ratio of the hysteresis loop exhibit a logarithmic decreasing trend with increasing cycle count under a constant dynamic stress amplitude in rocks such as siltstone, muddy siltstone, and fine sandstone. Conversely, under a fixed number of cycles, the hysteresis loop area increases exponentially with increasing stress amplitude, suggesting that the stress level plays a critical role in activating energy dissipation mechanisms. Moreover, the fitted relationships between the damping ratio, damping coefficient, and dynamic stress amplitude under varying cyclic conditions exhibit strong stability and predictive capability [46]. Overall, the evolution of rock damping properties is governed by the coupled influence of multiple factors, including the stress state, cyclic loading history, burial depth, diagenetic environment, and mineralogical composition.

Conclusions

1. Under the effect of graded cyclic loading, the damping ratio of Longmaxi shale clearly changes with the stress level. At the initial stage, as the stress amplitude increases, the microfissures inside the shale are compacted, and the energy dissipation gradually decreases, resulting in a decrease in the damping ratio. As the stress level continues to rise, the shale gradually enters an elastic dominant phase where the damping ratio stabilizes and increases slightly at higher stress levels.
2. Under cyclic loading, the shape of the radial hysteresis loop of the Longmaxi shale is similar to the characteristics of the axial hysteresis loop, indicating that the stress-strain hysteresis relationship is consistent in both directions. With increasing stress amplitude and number of cycles, plastic deformation and plastic strain energy gradually accumulate, resulting in the strain phase gradually exceeding the stress phase, resulting in a change in the hysteresis effect.
3. The radial damping ratio of the Longmaxi shale is consistently greater than the axial damping ratio under the same circumferential pressure and stress loading conditions, and this difference is particularly significant under high circumferential pressure conditions. This phenomenon is closely related to the anisotropy under high peripheral pressure conditions, and radial deformation is more constrained, resulting in more significant radial energy dissipation, which makes the radial damping ratio larger than the axial damping ratio, theropic characteristics of shale and the effect of peripheral pressure on fracture closure.
4. An increase in the peripheral pressure significantly affects the damping characteristics of the Longmaxi shale. Under the no-confining pressure condition, the mineral particles inside the shale are more loosely connected, which easily produces more significant plastic deformation, resulting in a narrower shape of the hysteresis loop and lower energy dissipation. As the confining pressure increases to 10 MPa, the slip between particles is restricted, the hysteresis loop gradually becomes full, and the damping ratio decreases. When the confining pressure further increases to 30 MPa, the cracks inside the shale begin to sprout and expand, resulting in an increase in energy dissipation and a significant increase in the damping ratio.

Data availability

If someone wants to request the data from this study， please contact the author Jiajun Shu.

Received: 16 March 2025; Accepted: 22 May 2025
Published online: 28 May 2025

References

1. Zhang, J. et al. Fields and directions for shale gas exploration in China. *Nat. Gas Ind. B* **9**(1), 20–32. https://doi.org/10.1016/j.ngib.2021.08.014 (2022).
2. He, X. et al. Deep shale gas exploration and development in the Southern Sichuan basin: New progress and challenges. *Nat. Gas Ind. B*. **10**(1), 32–43. https://doi.org/10.1016/j.ngib.2023.01.007 (2023).
3. Li, J. et al. Water quality deterioration of treated oilfield injection water in the water distribution system of the Jianghan oilfield. *Water Supply* **19**(2), 519–526. https://doi.org/10.2166/ws.2018.097 (2018).
4. Yu, X., Wang, C., Huang, H. & Yan, K. Origin of lithium in oilfield Brines in continental petroliferous basin: Insights from Li and Sr isotopes in the Jianghan basin, central China. *Mar. Petroleum Geol.* **160**, 106576. https://doi.org/10.1016/j.marpetgeo.2023.106576 (2024).
5. Zhou, Z. F., Wang, M. X., Zuo, X. H. & Yao, Y. H. Comparative investigation of bacterial, fungal, and archaeal community structures in soils in a typical oilfield in Jianghan, China. *Arch. Environ. Contam. Toxicol.* **72**(1), 65–77. https://doi.org/10.1007/s00244-016-0333-1 (2017).
6. Li, K. S., Yang, S. Q., Liu, C. X. & Song, Y. Mechanical response and energy evolution of interbedded shales subjected to multilevel constant/increasing-amplitude cyclic loading. *Can. Geotech. J.* **61**(11), 2485–2504. https://doi.org/10.1139/cgj-2023-0486 (2024).
7. Bajaj, K. & Anbazhagan, P. Identification of shear modulus reduction and damping curve for deep and shallow sites: Kik-Net data. *J. Earthq. Eng.* **25**(13), 2668–2696. https://doi.org/10.1080/13632469.2019.1643807 (2019).
8. Wang, H. et al. Deep and ultra-deep oil and gas well drilling technologies: Progress and prospect. *Nat. Gas Ind. B* **9**(2), 141–157. https://doi.org/10.1016/j.ngib.2021.08.019 (2022).
9. Habaraduwa Peellage, W., Fatahi, B. & Rasekh, H. Stiffness and damping characteristics of jointed rocks under Cyclic triaxial loading subjected to prolonged Cyclic loading. *Int. J. Fatigue* **181**, 108121. https://doi.org/10.1016/j.ijfatigue.2023.108121 (2024).
10. Wang, Y., Tang, P., Han, J. & Li, P. Influence of dynamic disturbed frequency on rock failure characteristics under triaxial cyclic and multistage unloading confining pressure loads. *Fatigue Fract. Eng. Mater. Struct.* **46**(4), 1527–1544. https://doi.org/10.1111/ffe.13946 (2023).

11. Yang, B. et al. Experimental investigation and empirical model on damping properties of rock under multistage cyclic loading. *Soil Dyn. Earthq. Eng.* **163**, 107557. https://doi.org/10.1016/j.soildyn.2022.107557 (2022).
12. Zhu, C., Zhao, J., Xue, J. & Lin, F. A simplified three-dimensional crack growth model to simulate the deformation of brittle rock under true triaxial stresses. *Eng. Fract. Mech.* **274**, 108784. https://doi.org/10.1016/j.engfracmech.2022.108784 (2022).
13. Li, C. et al. Rock physical characteristics of deep dolomite under complex geological conditions: A case study of 4th member of Sinian Dengying formation in the Sichuan basin, China. *Pet. Sci.* **21**(4), 2370–2382. https://doi.org/10.1016/j.petsci.2024.03.015 (2024).
14. Xu, J. et al. Experimental study of the damage characteristics of rocks containing non-penetrating cracks under cyclic loading. *Int. J. Min. Sci. Technol.* **34**(2), 197–210. https://doi.org/10.1016/j.ijmst.2024.02.002 (2024).
15. Zhang, W., Zhang, D., Guo, W. & Zhang, B. Experimental study on failure precursory characteristics and moisture content effect of pre-cracked rocks under graded cyclic loading and unloading. *Int. J. Min. Sci. Technol.* https://doi.org/10.1016/j.ijmst.2024.12.014 (2025).
16. Alpa, G. & Gambarotta, L. Theoretical evaluation of the frictional damping of rocks. *Int. J. Rock. Mech. Min. Sci. Geomech. Abstracts* **27**(4), 215. https://doi.org/10.1016/0148-9062(90)90681-q (1990).
17. Worthington, M. H., King, M. S. & Marsden, J. R. Determining the damping factor of sedimentary rocks required for seismically designed structures. *Int. J. Rock. Mech. Min. Sci.* **38**(6), 801–806. https://doi.org/10.1016/S1365-1609(01)00044-2 (2001).
18. Wu, Y. et al. Damping and stiffness responses of silica rock under constant amplitude and variable rate cyclic loading. *Appl. Sci.* **14**(11), 4713. https://doi.org/10.3390/app14114713 (2024).
19. Habaraduwa Peellage, W., Fatahi, B. & Rasekh, H. Assessment of Cyclic deformation and critical stress amplitude of jointed rocks via cyclic triaxial testing. *J. Rock. Mech. Geotech. Eng.* **15**(6), 1370–1390. https://doi.org/10.1016/j.jrmge.2023.02.001 (2023).
20. Angio, D., Lenti, L. & Martino, S. Microseismic monitoring to assess rock mass damaging through a novel damping ratio-based approach. *Int. J. Rock. Mech. Min. Sci.* **146**, 104883. https://doi.org/10.1016/j.ijrmms.2021.104883 (2021).
21. Deng, P., Liu, Q., Huang, X. & Ma, H. A new hysteretic damping model and application for the combined finite-discrete element method (FDEM). *Eng. Anal. Bound. Elem.* **132**, 370–382. https://doi.org/10.1016/j.enganabound.2021.08.021 (2021).
22. Wu, L. et al. Modeling and simulation of dynamic unloading of prestressed rock mass. *Comput. Model. Eng. Sci.* **120**(2), 421–443. https://doi.org/10.32604/cmes.2019.05218 (2019).
23. Farla, R. J. M., Jackson, I., Gerald, F., Faul, J. D., Zimmerman, U. H. & M. E Dislocation damping and anisotropic seismic wave attenuation in Earth's upper mantle. *Science* **336**(6079), 332–335. https://doi.org/10.1126/science.1218318 (2012).
24. Ding, X., Zhao, J. & Dong, Y. Dynamic properties and dynamic response model of jointed granites by cyclic loading. *Adv. Civil Eng.* **2024**(1). https://doi.org/10.1155/2024/7258680 (2024).
25. Al Atik, L., Gregor, N. J., Abrahamson, N. A. & Kottke, A. R. GMPE-consistent hard-rock site adjustment factors for Western North America. *Earthq. Spectra* **38**(4), 2371–2397. https://doi.org/10.1177/87552930221092467 (2022).
26. Sasaki, Y., Takei, Y., McCarthy, C. & Rudge, J. F. Experimental study of dislocation damping using a rock analogue. *J. Geophys. Res. Solid Earth*. **124**(7), 6523–6541. https://doi.org/10.1029/2018JB016906 (2019).
27. Shalev, E., Lyakhovsky, V., Simonin, A. O., Hamiel, Y. & Zhu, W. Inelastic compaction, dilation and hysteresis of sandstones under hydrostatic conditions. *Geophys. J. Int.* **197**(2), 920–925. https://doi.org/10.1093/gji/ggu052 (2014).
28. Liu, E. & He, S. Effects of cyclic dynamic loading on the mechanical properties of intact rock samples under confining pressure conditions. *Eng. Geol.* **125**, 81–91. https://doi.org/10.1016/j.enggeo.2011.11.007 (2012).
29. Li, N., Chen, W., Zhang, P. & Swoboda, G. The mechanical properties and a fatigue-damage model for jointed rock masses subjected to dynamic cyclical loading. *Int. J. Rock. Mech. Min. Sci.* **38**(7), 1071–1079. https://doi.org/10.1016/S1365-1609(01)00058-2 (2001).
30. Wang, Y., Han, J., Li, P. & Cai, M. Effect of prior cyclic damage on rock failure exposed to triaxial multistage unloading confining pressure and cyclic loads. *Fatigue Fract. Eng. Mater. Struct.* **46**(3), 1140–1158. https://doi.org/10.1111/ffe.13926 (2023).
31. Wang, K., Pan, D., Lu, W. & Chen, F. Experimental study on damping characteristics of mudstone and sandstone under graded cyclic loading. *J. Cent. South. Univ. (Science Technology)* **50**(12), 3046–3054. https://doi.org/10.11817/j.issn.1672-7207.2019.12.014 (2019).
32. David, E. C., Brantut, N. & Hirth, G. Sliding crack model for nonlinearity and hysteresis in the triaxial stress-strain curve of rock, and application to Antigorite deformation. *J. Geophys. Res. Solid Earth* **125**(10). https://doi.org/10.1029/2019JB018970 (2020).
33. Liu, H. et al. Strength and damage evolution mechanism of rock mass with holes under cyclic loading. *J. Cent. South. Univ.* **31**, 2717–2735. https://doi.org/10.1007/s11771-024-5714-4 (2024).
34. Wang, H. et al. Experimental investigation of linear damping characteristics on granite and red sandstone under dynamic cyclic loading. *Eur. J. Environ. Civil Eng.* **26**(11), 5259–5278. https://doi.org/10.1080/19648189.2021.1902715 (2022).
35. Yang, B., He, M., Zhang, Z., Zhu, J. & Chen, Y. Experimental investigation and empirical model on damping properties of rock under multistage Cyclic loading. *Soil Dyn. Earthq. Eng.* **163**, 107557. https://doi.org/10.1016/j.soildyn.2022.107557 (2022).
36. Xu, H., Quan, Z. Y., Liu, J. P., Jiang, X. H. & Cheng, F. Study on the propagation characteristics of seismic waves perpendicular to the earth-rock dam axis. *Soil Dyn. Earthq. Eng.* **186**, 108907. https://doi.org/10.1016/j.soildyn.2023.108907 (2024).
37. Jiang, C. et al. Study on deformation characteristics and energy evolution mechanism of shale under constant amplitude cyclic loading. *J. Rock. Mech. Eng.* **39**(12), 2416–2428 (2020). (**in Chinese**).
38. Jiang, C. et al. Study on hysteresis effect and damping characteristics of shale under saturated and natural conditions. *Geotech. Mech.* **41**(6), 1799–1808. https://doi.org/10.13722/j.gds.2020.06.005 (2021).
39. Peellage, W. H., Behzad, F. & Rasekh, H. Assessment of cyclic deformation and critical stress amplitude of jointed rocks via cyclic triaxial testing. *J. Rock. Mech. Geotech. Eng.* **15**(6), 1370–1390. https://doi.org/10.1016/j.jrmge.2023.04.012 (2023).
40. Dai, S. et al. Failure criterion of submarine completely weathered granite under cyclic loads in rock-based sea area. *Ocean Eng.* **313**, 119422. https://doi.org/10.1016/j.oceaneng.2024.119422 (2024).
41. Peellage, W. H., Behzad, F. & Rasekh, H. Experimental investigation for vibration characteristics of jointed rocks using cyclic triaxial tests. *Soil Dyn. Earthq. Eng.* **160**, 107377 (2022). https://doi.org/10.1016/j.soildyn.2022.107377
42. Xi, D., Xu, S., Xi, J., Yi, L. & Du, Y. Experimental study on viscoelastic behavior of saturated sandstone. *Chin. J. Geophys.* **54**(9), 2302–2308 (2011). (**in Chinese**).
43. Yang, B., He, M. & Chen, Y. Experimental study of nonlinear damping characteristics on granite and red sandstone under the multi-level cyclic loading-unloading triaxial compression. *Arab. J. Geosci.* **13**(2). https://doi.org/10.1007/s12517-019-5022-8 (2020).
44. Wang, K., Pan, D., Lu, W. & Chen, F. Experimental study on damping properties of mudstone and sandstone under graded Cyclic loading. *J. Cent. South. Univ.* **50**(12), 3046–3054 (2019). (**in Chinese**).

Acknowledgements

This research acknowledges the financial support provided by the National Natural Science Foundation of China (Grant NO. 51508556), Natural Science Foundation of Jiangxi Province (Grant NO. 20232BAB203079 and Grant NO. 20224BAB213045), China University of Mining and Technology-Beijing Inner Mongolia Research Institute Foundation (IMRI23009), Program of China Scholarship Council (Grant NO. 202406430056).

Author contributions

Jiajun Shu: Writing-original draft, Administration. Tao Li: Writing-review & editing, Data curation, Investigation, Funding acquisition. Yue Li: Data curation, Administration. Bingni Wu: Methodology, Super vision. Zhengding Deng: Writing-review & editing, Funding acquisition. Jingzhu Huang: Visualization, Data curation. Rubén Galindo: Writing—review & editing, Visualization, Data curation. Fausto Molina Gómez: Writing—review & editing.

Declarations

Competing interests

The authors declare no competing interests.

Additional information

Correspondence and requests for materials should be addressed to J.S., T.L. or R.G.

Reprints and permissions information is available at www.nature.com/reprints.

Publisher's note Springer Nature remains neutral with regard to jurisdictional claims in published maps and institutional affiliations.